



TITLE:

Synthetic RNA-protein complex
shaped like an equilateral triangle.

AUTHOR(S):

Ohno, Hirohisa; Kobayashi, Tetsuhiro; Kabata,
Rinko; Endo, Kei; Iwasa, Takuma; Yoshimura, Shige
H; Takeyasu, Kunio; Inoue, Tan; Saito, Hirohide

CITATION:

Ohno, Hirohisa ...[et al]. Synthetic RNA-protein complex shaped like an
equilateral triangle.. Nature nanotechnology 2011, 6(2): 116-120

ISSUE DATE:

2011-01-16

URL:

<http://hdl.handle.net/2433/197491>

RIGHT:

© 2011 Macmillan Publishers Limited.; この論文は出版社版でありませ
ん。引用の際には出版社版をご確認ご利用ください。; This is not the
published version. Please cite only the published version.

Synthetic RNA-protein complex shaped like an equilateral triangle

Hirohisa Ohno¹, Tetsuhiro Kobayashi¹, Rinko Kabata¹, Kei Endo², Takuma Iwasa¹, Shige H. Yoshimura³, Kunio Takeyasu³, Tan Inoue^{1,2,*} and Hirohide Saito^{1,2,4*}

delete

1 Synthetic nanostructures consisting of biomacromolecules such as nucleic acids have been constructed using bottom-up approaches^{1,2}. In particular, Watson-Crick base pairing has been used to construct a variety of two- and three-dimensional DNA nanostructures³⁻¹⁰. Here, we show that RNA and the ribosomal protein L7Ae can form a nanostructure shaped like an equilateral triangle that consists of three proteins bound to an RNA scaffold. The construction of the complex relies on the proteins binding to kink-turn (K-turn) motifs in the RNA¹¹⁻¹³, which allows the RNA to bend by $\sim 60^\circ$ at three positions to form a triangle. Functional RNA-protein complexes constructed with this approach could have applications in nanomedicine^{14,15} and synthetic biology^{14,16-18}.

RNA can be used to design and build synthetic nanoscale objects through a combination of naturally occurring structural motifs and non-Watson-Crick motifs such as loop-receptor-interacting motifs¹⁹, three-way junctions²⁰ and K-turn motifs^{21,22}. For example, synthetic RNA enzymes (ribozymes) have been designed and developed by combining molecular design and *in vitro* evolution techniques with RNA scaffolds that have been computationally designed and catalytic cores that are obtained from a pool of random sequences²³⁻²⁵. However, it is difficult to produce a variety of ribozymes and complex nanostructures using RNA alone²⁶⁻³⁰, and this has led to interest in the use of RNA-protein

complexes (RNPs). Here, we use the interaction between the box C/D K-turn motif in RNA and the K-turn binding protein L7Ae as a building element^{11-13,31} to design and synthesize a triangular RNP. Atomic force microscopy (AFM) revealed that L7Ae induces a conformational alteration in the designed RNAs to form the triangular RNP objects.

We chose L7Ae and the box C/D K-turn (box C/D_{mini}) because they associate with high affinity, specificity and stability (Supplementary Fig. S1 and text). We designed an RNP nanostructure containing three box C/D_{mini} motifs and three L7Ae proteins (Fig. 1a,b). The box C/D_{mini} K-turn RNA, which is relatively flexible by itself, is bent to fix the bending angle of the K-turn at $\sim 60^\circ$ by binding to L7Ae (Fig. 1a)¹³; we refer to this nanostructure as 'Tri-RNP' (triangular-shaped RNP). The Tri-RNP-1 (Fig. 1b) was designed to have one side with a length of 16.7 nm (including both the double-stranded RNA (dsRNA) and L7Ae). The dsRNA region was flanked by the box C/D_{mini} K-turn motifs to form three apices (Supplementary Fig. S2a). L7Ae could facilitate the formation of triangle-like RNPs by stabilizing the K-turn regions with an angle of $\sim 60^\circ$ between the axes, whereas the dsRNA by itself could present heterogeneous RNA structures due to the flexibility of the K-turn (Fig. 1c).

Two complementary RNAs (large (L-1)- and short (S-1)-strand RNAs) were prepared and hybridized to generate LS-1 RNA

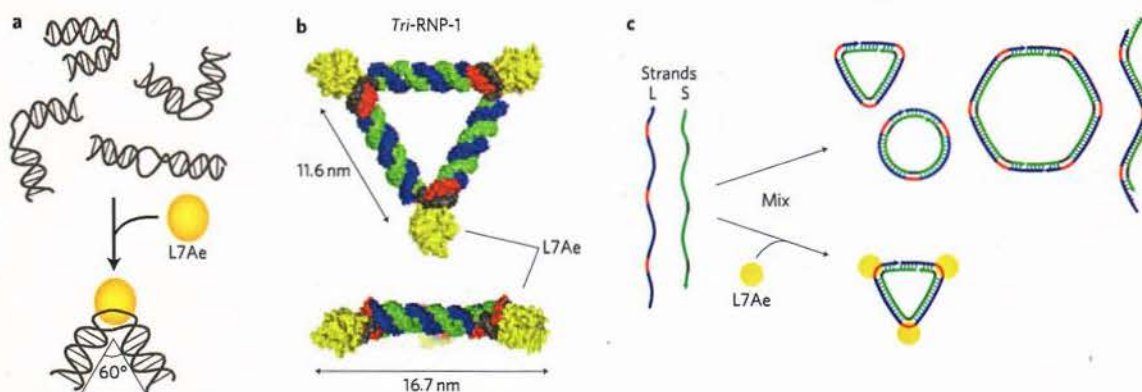


Figure 1 | Molecular design of the triangular RNP (Tri-RNP). **a**, Induced-fit interaction between L7Ae and the K-turn RNA motif. **b**, Three-dimensional model of Tri-RNP-1 composed of two RNA strands (the L-1 strand is shown in blue and red, the S-1 strand in green and grey) and three L7Ae proteins (yellow). Three K-turn regions can be observed (red and grey). **c**, Schematic representation of the triangular RNP formation. In the absence of L7Ae, two RNAs form heterogeneous structures, including triangular, linear, circular or multimer forms composed of sets of L/S strands. In the presence of L7Ae, the three K-turn regions are fixed at $\sim 60^\circ$, which facilitates the formation of the designed triangular RNP.

¹Laboratory of Gene Biodynamics, Graduate School of Biostudies, Kyoto University, Oiwake-cho, Kitashirakawa, Sakyo-ku, Kyoto, 606-8502, Japan,

²International Cooperative Research Project (ICORP), Japan Science and Technology Agency (JST), 5 Sanban-cho, Chiyoda-ku, Tokyo 102-0075, Japan,

³Laboratory of Plasma Membrane and Nuclear Signaling, Graduate School of Biostudies, Kyoto University, Japan, ⁴The Hakubi Center, Kyoto University, Japan. *e-mail: saito@lif.kyoto-u.ac.jp; tan@kuchem.kyoto-u.ac.jp

LETTERS

NATURE NANOTECHNOLOGY DOI: 10.1038/NNANO.2010.268

(Supplementary Fig. S2b). Electrophoretic mobility gel shift assay (EMSA) revealed that the L-1 and S-1 RNAs effectively interacted with one another to form the LS-1 RNA (Fig. 2, lanes 2–4). The LS-1 RNA (final concentration, 50 nM), which contained three K-turn motifs, interacted with L7Ae in a concentration-dependent manner (Fig. 2, lanes 5–9), indicating that L7Ae specifically associated with K-turn motifs of LS-1 RNA. Three bands were seen to move more slowly (that is, shifted up) in the presence of the different concentrations of L7Ae (Fig. 2, lanes 7–9), implying that the three L7Ae proteins interacted with the three box C/D_{mini} motifs in the RNA in the presence of excess L7Ae (Fig. 2). A derivative of the skeletal RNA (LS-1 RNA_{mut}) (Supplementary Fig. S1b) resulted in an impaired shift (Supplementary Fig. S3a). A derivative of L7Ae (L7AeK37K79A; L7AeKK_{mut}) with a weaker affinity to box C/D_{mini} also failed to yield the shifted band under the conditions we used (Supplementary Fig. S3b). Thus, it is conceivable that the skeletal RNA with K-turn motifs selectively interacts with L7Ae to form an RNP.

We next analysed the structure of the RNP using AFM (Supplementary Fig. S4). In the absence of L7Ae, heterogeneous RNA structures (for example, circular, linear, triangle-like or elliptical) were observed, presumably due to the flexible K-turn structures in LS-1 RNA (Fig. 3a, left; Supplementary Fig. S5, top). As expected, the number of triangular RNPs increased in the presence of L7Ae (Fig. 3a, middle; Fig. 3b; Supplementary Fig. S5, middle). Furthermore, the numbers of multimers (doughnut-like shapes) and linear RNA structures were reduced in the presence of L7Ae (Fig. 3a; Supplementary Fig. S5, top versus middle). AFM analyses confirmed that the facilitated formation of the triangular structures was due to the presence of both LS-1 RNA and L7Ae (Fig. 3a). In contrast, LS-1 RNA_{mut}, which contains the heterogeneous RNA structures, did not form the triangular shape in the presence of L7Ae (Supplementary Fig. S6). Similarly, fewer structural conversions were observed for the mixture of LS-1 RNA and L7AeKK_{mut} (Supplementary Fig. S5, bottom). These results indicate that L7Ae induces a structural alteration of the LS-1 RNA into a triangular form by binding to K-turn motifs.

The sizes of the observed triangular shapes and the other objects (Supplementary Fig. S5) were determined by measuring the longest side of each object. The average length of the triangular objects was 21.7 ± 1.1 nm or 24.6 ± 1.5 nm (Fig. 3c; Supplementary Fig. S5) in the absence or presence of L7Ae, respectively, indicating the formation of the designed nanoscale RNP objects (see Supplementary Fig. S4 for the observed size of *Tri*-RNP-1). The average height of the object in the presence of L7Ae was ~ 1.5 nm, which was consistent with the height of the RNA duplexes on a mica surface²⁷.

To investigate whether the lengths of the three sides of each triangular object were close to identical, the standard deviation of the three side lengths of each object (coefficient of variation of the three side lengths; 44 objects in total) was determined. The majority of the objects turned out to have an equilateral-triangle shape (Supplementary Fig. S7), allowing us to assume that the actual RNP architectures were close to the designed ones.

To construct a variant *Tri*-RNP, we designed a large triangular RNP, termed *Tri*-RNP-2, with 48 bp on one side (Supplementary Figs S8 and S9) and a predicted length of 22.6 nm, including dsRNA and L7Ae (Supplementary Fig. S4). As for *Tri*-RNP-1, EMSA confirmed that the skeletal *Tri*-RNP-2 interacted with L7Ae (Supplementary Fig. S10a). L7AeKK_{mut} exhibited no interaction with the RNA under these conditions (Supplementary Fig. S10b). Furthermore, EMSA and size-exclusion chromatography revealed that the *Tri*-RNP-2 was larger than the *Tri*-RNP-1, as designed (Supplementary Figs S11 and S12).

After size-exclusion chromatography to purify the *Tri*-RNP complexes, we measured the sizes of *Tri*-RNP-1 and *Tri*-RNP-2 using AFM. As expected, RNP-1 and RNP-2 triangular forms

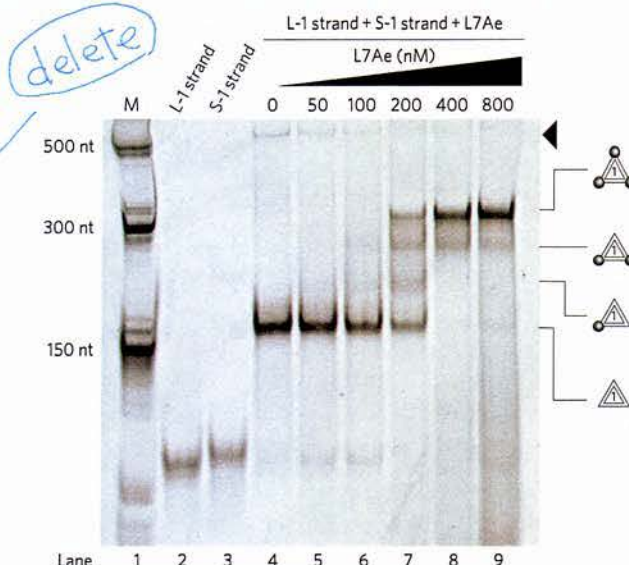


Figure 2 | Interaction between the RNA and the protein. Interaction between L7Ae and the RNA designed to contain three box C/D_{mini} motifs was analysed by EMSA. LS-1 RNA was assayed in the presence of increasing amounts of L7Ae (lanes 4–9). Three upshifted bands were observed in lanes 5–9, indicating the formation of RNP complexes that contain one, two or three L7Ae, respectively. The upper band (indicated by the black arrowhead), corresponding to the heterogeneous LS-1 RNA structures, was reduced in the presence of L7Ae, suggesting either that L7Ae induced structural conversion of LS-1 RNA towards one particular form, or heterogeneous RNAs interacting with L7Ae shifted the band to the gel slot. Lane 1, single-stranded RNA marker; lane 2, L-1 RNA; lane 3, S-1 RNA; lane 4, LS-1 RNA.

were observed (Fig. 4a). The average and longest side lengths of *Tri*-RNP-2 (27.5 and 29.4 nm, respectively) were longer than those of *Tri*-RNP-1 (21.3 and 23.1 nm, respectively) (Fig. 4b). The coefficient of variation of the lengths of the three sides of *Tri*-RNP-2 strongly indicated that most of the triangular objects were equilateral-triangular (Supplementary Fig. S13), demonstrating that the molecular design of *Tri*-RNP with different dimensions is feasible.

The effect of metal ions on the formation of *Tri*-RNP-2 was then examined. AFM indicated that a certain portion of LS-2 RNA formed a triangle-like structure in the absence of L7Ae under our EMSA conditions (1.5 mM MgCl₂ and 150 mM KCl). However, the number of such triangular RNAs was reduced significantly, and the number of linear and circular RNAs increased, in the presence of lower concentrations of metal ions (no MgCl₂ and 30 mM KCl) (Fig. 4c, top). The addition of L7Ae facilitated the conversion of LS-2 RNA into the triangular structure (Fig. 4c, bottom). This result is consistent with previous findings that the formation of the K-turn structure depends on the concentrations of metal ions and L7Ae^{13,32}.

Finally, we attempted to attach functional proteins to the three vertices of the triangular RNA scaffold (Supplementary Fig. S14a). EMSA and AFM analyses confirmed that three L7Ae-EGFP proteins effectively interacted with the RNA complex to form the triangular objects (Supplementary Fig. S14b–d). To investigate the stability and versatility of the RNA triangle containing functional proteins, the interactions were analysed by EMSA under physiological conditions (PBS or Opti-MEM) (Supplementary Fig. S15). The tested interactions between the RNA and the proteins (L7Ae, L7Ae-EYFP or L7Ae-GB1) confirmed that the RNP complexes under these physiological conditions are as stable as those under our RNP binding condition.

Q10

Q2

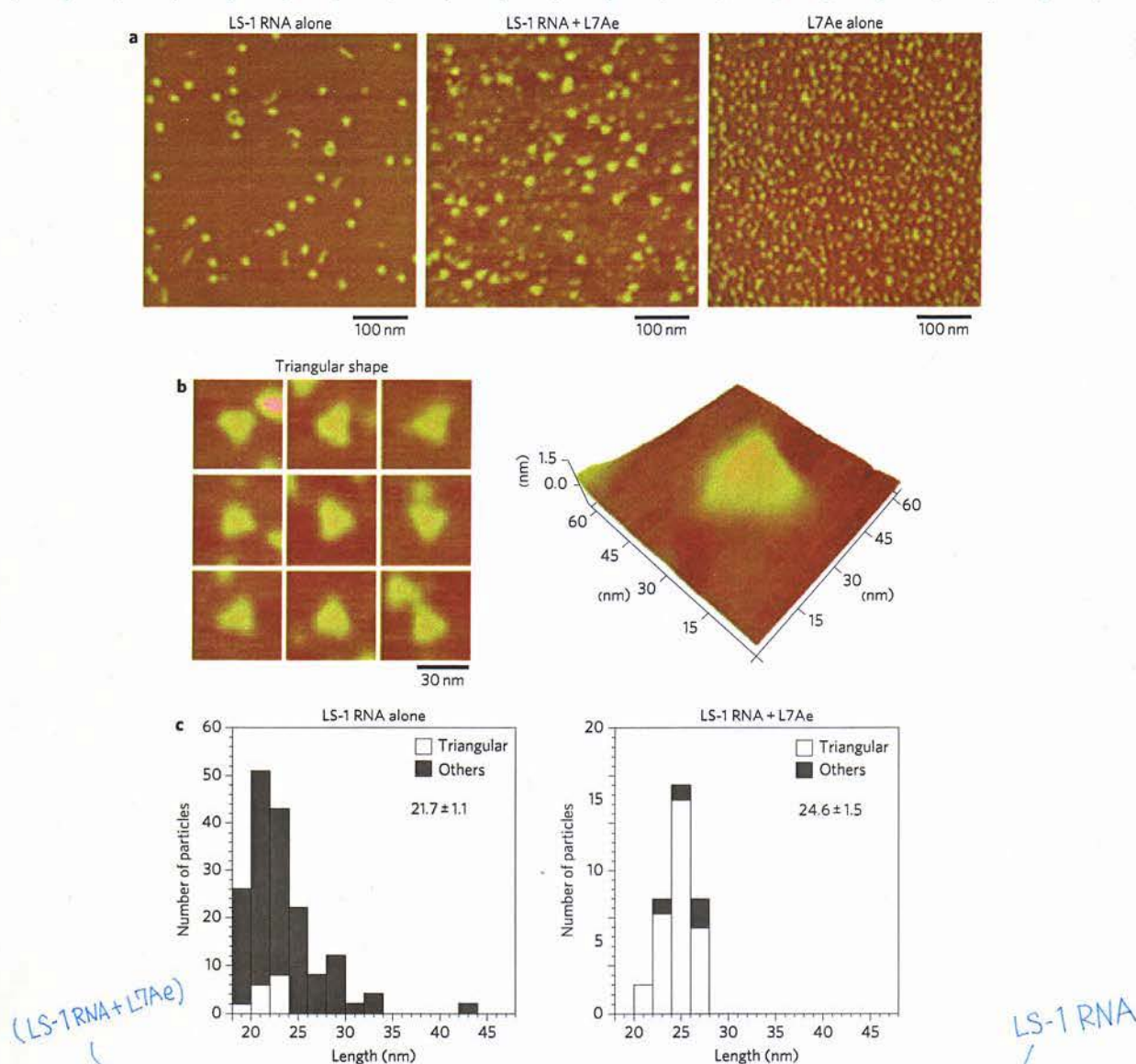


Figure 3 | AFM imaging of *Tri*-RNP-1. **a**, AFM images of LS-1 RNA only (left), LS-1 RNA with L7Ae (middle) and L7Ae alone (right). **b**, Left: magnified images of *Tri*-RNP-1 showing triangular structures. Right: three-dimensional image of *Tri*-RNP-1. **c**, Distributions of the dimensions of *Tri*-RNP-1 in the absence (left) or presence (right) of L7Ae. White and grey bars indicate data for the triangular and other-shaped RNPs, respectively. The average lengths of the longest side of the observed triangular RNA object in the absence and presence of L7Ae were 21.7 ± 1.1 and 24.6 ± 1.5 nm, respectively. Note that although the designed *Tri*-RNP-1 had a length of 16.7 nm, the tip effect of the AFM suggested that the observed size would be ~ 24 nm (Supplementary Fig. S4).

We have demonstrated that RNP can be used to design and construct nanoscale triangular structures. Three proteins can be attached to the apices of the RNA triangle to minimize steric hindrance between the proteins; the rigid RNA rods physically separate the proteins. This RNP design could potentially form a multifunctional agent for biological applications^{14,33}. For example, the triangular RNP could be used for controlling cellular signalling by means of some cell surface receptors (for example, tumour necrosis factor receptors) known to function as a trimer; certain receptors send signals only when trimerized or oligomerized^{34,35}. The relative orientation of the three components of the receptors could be fixed by the cognate three ligands at the three apices of the resizable RNP. Thus, the RNP triangle could be used as a potent agonist or antagonist for this application. Moreover, because RNA can be transcribed in cells, RNP nanostructures that are produced *in vivo* will be usable in regulating biological functions in cells. In addition to

the L7Ae K-turn structure, many other high-resolution structures of RNP are known, including ribosomes and other ribozymes^{17,36}. Incorporation of their numerous RNP motifs in nano-architecture will significantly expand the repertoire of designable and usable nanosized molecules. In contrast to DNA nanotechnology, which relies on Watson-Crick base pairing³⁻¹⁰ to build nanostructures, our strategy using proteins to induce structural changes is advantageous, because it may be possible to construct RNA-protein complexes with functionalities comparable to ribosomes.

Methods

Molecular design of triangular RNPs. The three-dimensional atomic model of L7Ae-box C/D K-turn was obtained from PDB (ID: 1RLG). Two bromo-uridines in the model were substituted to uridines, and an energy minimization protocol was adapted. This modified L7Ae-K-turn structural model was used to design triangular RNPs (*Tri*-RNP-1 and *Tri*-RNP-2) as follows. Three identical L7Ae-K-turn motifs were connected by three linear RNA double helices (each containing 24 or 48

LETTERS

NATURE NANOTECHNOLOGY DOI: 10.1038/NNANO.2010.268

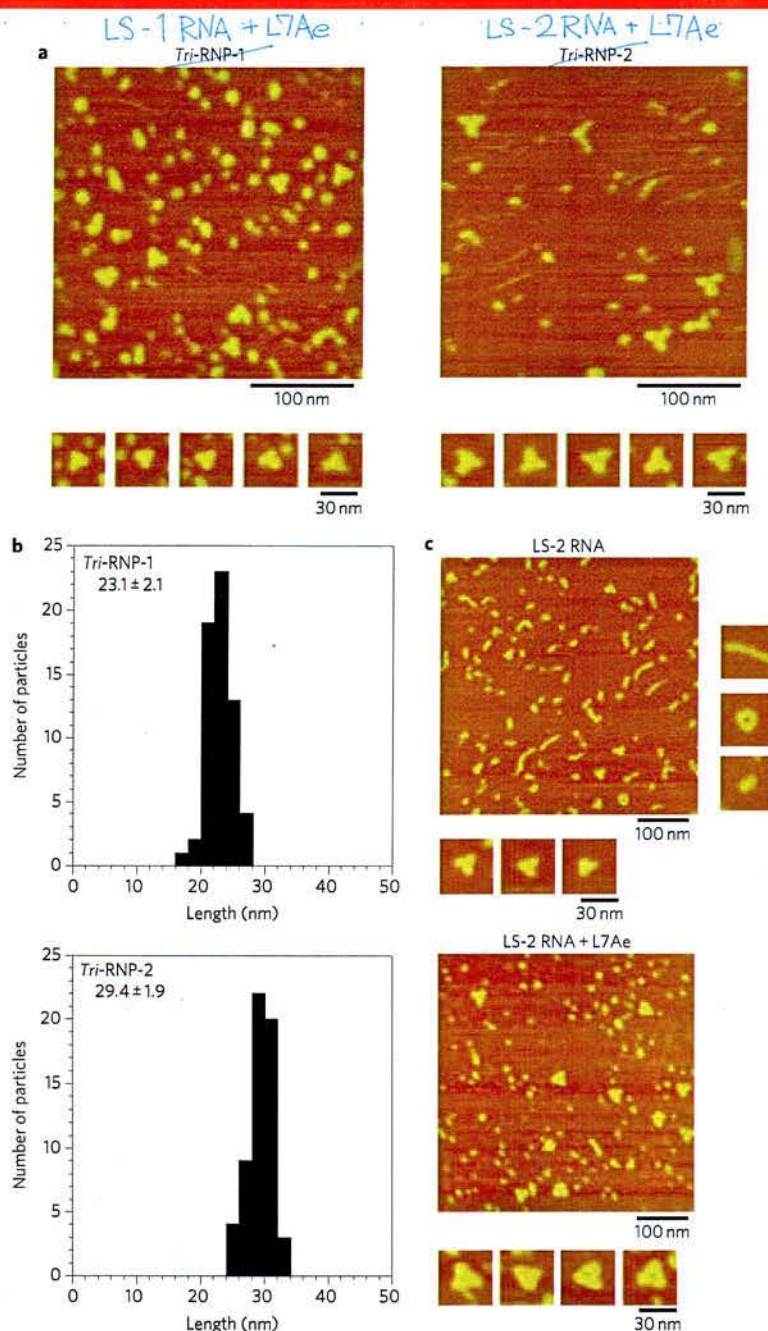


Figure 4 | Comparison of the dimensions of *Tri*-RNP-1 and *Tri*-RNP-2. **a, AFM images of LS-1 or LS-2 RNA with L7Ae. Images of the triangles are also shown in the lower panels. **b**, Sizes of the purified *Tri*-RNP-1 and *Tri*-RNP-2 analysed by AFM. The average lengths of the longest side of each of the observed triangular objects (*Tri*-RNP-1 and *Tri*-RNP-2) were 23.1 ± 2.1 and 29.4 ± 1.9 nm, respectively. **c**, Top, the absence of L7Ae and lower concentrations of metal ions (no $MgCl_2$ and 30 mM KCl) resulted in linear and circular RNAs and fewer triangles. Bottom, the addition of L7Ae facilitated the formation of triangular structures.**

1 Watson-Crick base pairs for *Tri*-RNP-1 or *Tri*-RNP-2, respectively) to form an
2 equilateral triangle. To check the suitability of the conformation, the *Tri*-RNP
3 structure was compared with the energy-minimized structure. We confirmed the
4 lack of significant structural differences between the two structures, indicating that
5 the designed model was relatively stable. Molecular designs and simulations were
6 performed with Discovery Studio (Accelrys). To ensure that the three double-helix
7 regions selectively formed the designed secondary structure, the sequences of the
8 DNA tetrahedral nanostructure were used³.
9 **DNA and RNA preparations.** All DNA templates and primers used in this study
10 were purchased from Hokkaido System Science or Greiner Japan (Supplementary
11 Table 1). The minimal box C/D motif (box C/D_{mini}) at the three vertices of the
12 triangle was prepared based on the sequence from *Archaeoglobus fulgidus*¹³. DNA

templates for *in vitro* transcription were generated by polymerase chain reaction
(PCR) with KOD-plus DNA polymerase (Toyobo). All RNA molecules were
transcribed *in vitro* by a MEGAshortscript kit (Ambion). To purify the transcripts,
denaturing polyacrylamide gel electrophoresis (PAGE) was performed. After the
recovery of RNAs, their concentrations were measured in a NanoDrop (Thermo
Scientific).

Protein preparation. L7Ae and its mutant (L7AeK37K79A) were prepared as
described previously^{12,31}. Briefly, the pET 28-b+ vector (Novagen) was selected for
the cloning and expression of the recombinant protein L7Ae from *A. fulgidus*. The
plasmid (pET 28-b+ -L7Ae) was transformed into *E. coli* BL-21 (DE3) (pLysS)
cells. Protein expression was induced with 1 mM IPTG, and the culture was
incubated overnight at 30 °C. The cells were harvested by centrifugation at

Q11

Q4

- 1 6,000 r.p.m. for 20 min at 4 °C and resuspended in sonication buffer (50 mM
2 phosphate buffer, pH 8.0, 300 mM NaCl) at 4 °C. The suspension was sonicated,
3 and the lysate incubated for 15 min at 80 °C to denature endogenous protein, which
4 was removed by centrifugation at 6,000 r.p.m. for 20 min at 4 °C. The supernatant
5 contained the recombinant hexahistidine-tagged L7Ae protein. L7Ae was purified
6 from the supernatant using Ni-NTA agarose following the manufacturer's directions
7 (Qiagen). The purity of the protein was confirmed by sodium dodecyl sulphate
8 (SDS)-PAGE. The eluted protein was concentrated using a YM-3 microcon
9 (Millipore), and dialysed against buffer containing 20 mM HEPES-KOH (pH 7.5),
10 150 mM KCl, 1.5 mM MgCl₂ and 5% glycerol. The concentration of the purified
11 L7Ae protein was determined using the Bradford protein assay (Bio-Rad). The
12 purified L7Ae protein was stored in storage buffer (20 mM HEPES-KOH (pH 7.4),
13 150 mM KCl, 1.5 mM MgCl₂ containing 40% glycerol) at -20 °C.
- 14 **Electrophoretic mobility shift assay (EMSA).** Mixtures of 0.5 µl each of L-1 or L-2
15 and S-1 or S-2 RNA (final concentration, 50 nM), 2 µl of 5× binding buffer (final
16 concentrations, 20 mM HEPES-KOH (pH 7.5), 150 mM KCl, 1.5 mM MgCl₂,
17 2 mM DTT, 3% glycerol) and 6 µl of Milli-Q water were heated at 80 °C for 3 min
18 and then cooled at room temperature for 10–30 min to fold LS-1 or LS-2 RNA.
19 After the addition of 1 µl of 10× L7Ae solution, mixtures were kept at room
20 temperature for 10 min to allow binding of the RNA and L7Ae. Mixtures added to
21 1 µl of dye (0.25% bromophenol blue (BPP), 0.25% xylene cyanol (XC), 30%
22 glycerol) were run in a native polyacrylamide gel with 0.5× TBE either at room
23 temperature or at 4 °C. After electrophoresis, gels were stained with SYBR Green II
24 (Molecular Probes) and observed using FLA-3000/7000 (Fujifilm). Between 0.8 and
25 5 µM of L7Ae, no significant difference was observed in the gel-shift of RNP. An
26 excess amount of L7Ae (~400 nM) was required for full-binding to LS-RNA
27 (50 nM) under our tested EMSA conditions, probably due to a folding problem in
28 the K-turn structures.
- 29 **Atomic force microscopy.** Observations were performed in air. RNA and/or
30 protein samples were prepared as described for EMSA. A fresh mica surface was
31 coated with 10 mM spermidine. The prepared samples (50 nM RNA with or without
32 1 µM L7Ae) diluted with water (~10- to 20-fold) were applied onto the mica for
33 ~10 min, rinsed with 1 ml water, and dried by blowing with N₂. The specimen was
34 observed using a NanoScope IIIa (Veeco) equipped with a type E scanner and a
35 cantilever made of silicon nitride (OMCL-AC160TS; Olympus) in tapping mode.
36 AFM images were analysed with the software accompanying the imaging unit
37 (Veeco).
- 38 Received 26 July 2010; accepted 7 December 2010;
39 published online XX XX 2010
- 40 **References**
- 41 1. Seeman, N. C. Nanomaterials based on DNA. *Annu. Rev. Biochem.* **79**,
42 65–87 (2010).
- 43 2. Lin, C., Liu, Y. & Yan, H. Designer DNA nanoarchitectures. *Biochemistry*
44 **48** (2009).
- 45 3. Goodman, R. P. *et al.* Rapid chiral assembly of rigid DNA building blocks for
46 molecular nanofabrication. *Science* **310**, 1661–1665 (2005).
- 47 4. Rothmund, P. W. Folding DNA to create nanoscale shapes and patterns. *Nature*
48 **440**, 297–302 (2006).
- 49 5. Andersen, E. S. *et al.* Self-assembly of a nanoscale DNA box with a controllable
50 lid. *Nature* **459**, 73–76 (2009).
- 51 6. Douglas, S. M. *et al.* Self-assembly of DNA into nanoscale three-dimensional
52 shapes. *Nature* **459**, 414–418 (2009).
- 53 7. Rinker, S., Ke, Y., Liu, Y., Chhabra, R. & Yan, H. Self-assembled DNA
54 nanostructures for distance-dependent multivalent ligand–protein binding.
55 *Nature Nanotech.* **3**, 418–422 (2008).
- 56 8. Ke, Y., Lindsay, S., Chang, Y., Liu, Y. & Yan, H. Self-assembled water-soluble
57 nucleic acid probe tiles for label-free RNA hybridization assays. *Science* **319**,
58 180–183 (2008).
- 59 9. Voigt, N. V. *et al.* Single-molecule chemical reactions on DNA origami. *Nature*
60 *Nanotech.* **5**, 200–203 (2010).
- 61 10. Endo, M., Katsuda, Y., Hidaka, K. & Sugiyama, H. Regulation of DNA
62 methylation using different tensions of double strands constructed in a defined
63 DNA nanostructure. *J. Am. Chem. Soc.* **132**, 1592–1597 (2010).
- 64 11. Moore, T., Zhang, Y., Fenley, M. O. & Li, H. Molecular basis of box C/D
65 RNA–protein interactions; cocrystal structure of archaeal L7Ae and a box C/D
66 RNA. *Structure* **12**, 807–818 (2004).
- 67 12. Rozhddestvensky, T. S. *et al.* Binding of L7Ae protein to the K-turn of archaeal
68 snoRNAs: a shared RNA binding motif for C/D and H/ACA box snoRNAs
69 in Archaea. *Nucleic Acids Res.* **31**, 869–877 (2003).
- 70 13. Turner, B., Melcher, S. E., Wilson, T. J., Norman, D. G. & Lilley, D. M. Induced
71 fit of RNA on binding the L7Ae protein to the kink-turn motif. *RNA* **11**,
1192–1200 (2005).
- 72 14. Guo, P. RNA nanotechnology: engineering, assembly and applications in
73 detection, gene delivery and therapy. *J. Nanosci. Nanotechnol.* **5**,
1964–1982 (2005).
- 74 15. Guo, P. The emerging field of RNA nanotechnology. *Nature Nanotech.* **5** (2010).
- 75 16. Saito, H. & Inoue, T. Synthetic biology with RNA motifs. *Int. J. Biochem. Cell*
76 *Biol.* **41**, 398–404 (2009).
- 77 17. Saito, H. & Inoue, T. RNA and RNP as new molecular parts in synthetic biology.
78 *J. Biotechnol.* **132**, 1–7 (2007).
- 79 18. Win, M. N., Liang, J. C. & Smolke, C. D. Frameworks for programming
80 biological function through RNA parts and devices. *Chem. Biol.*
81 **16**, 298–310 (2009).
- 82 19. Jaeger, L. & Chworos, A. The architectonics of programmable RNA and DNA
83 nanostructures. *Curr. Opin. Struct. Biol.* **16**, 531–543 (2006).
- 84 20. Leontis, N. B., Lescoute, A. & Westhof, E. The building blocks and motifs of
85 RNA architecture. *Curr. Opin. Struct. Biol.* **16**, 279–287 (2006).
- 86 21. Matsumura, S., Ikawa, Y. & Inoue, T. Biochemical characterization of the
87 kink-turn RNA motif. *Nucleic Acids Res.* **31**, 5544–5551 (2003).
- 88 22. Lescoute, A., Leontis, N. B., Massire, C. & Westhof, E. Recurrent structural RNA
89 motifs, isostericity matrices and sequence alignments. *Nucleic Acids Res.*
90 **33** (2005).
- 91 23. Ikawa, Y., Tsuda, K., Matsumura, S. & Inoue, T. *De novo* synthesis and
92 development of an RNA enzyme. *Proc. Natl Acad. Sci. USA* **101**,
13750–13755 (2004).
- 93 24. Penchovsky, R. & Breaker, R. R. Computational design and experimental
94 validation of oligonucleotide-sensing allosteric ribozymes. *Nature Biotechnol.*
95 **23**, 1424–1433 (2005).
- 96 25. Voytek, S. B. & Joyce, G. F. Niche partitioning in the coevolution of 2 distinct
97 RNA enzymes. *Proc. Natl Acad. Sci. USA* **106**, 7780–7785 (2009).
- 98 26. Horiya, S. *et al.* RNA LEGO: magnesium-dependent formation of specific RNA
99 assemblies through kissing interactions. *Chem. Biol.* **10**, 645–654 (2003).
- 100 27. Chworos, A. *et al.* Building programmable jigsaw puzzles with RNA. *Science*
101 **306**, 2068–2072 (2004).
- 102 28. Ko, S. H., Chen, Y., Shu, D., Guo, P. & Mao, C. Reversible switching of pRNA
103 activity on the DNA packaging motor of bacteriophage phi29. *J. Am. Chem. Soc.*
104 **130**, 17684–17687 (2008).
- 105 29. Severcan, I. *et al.* A polyhedron made of tRNAs. *Nature Chem.* **2**,
772–779 (2010).
- 106 30. Afonin, K. A. *et al.* *In vitro* assembly of cubic RNA-based scaffolds designed in
107 silico. *Nature Nanotech.* **5**, 676–682 (2010).
- 108 31. Saito, H. *et al.* Synthetic translational regulation by an L7Ae-kink-turn RNP
109 switch. *Nature Chem. Biol.* **6**, 71–78 (2010).
- 110 32. Goody, T. A., Melcher, S. E., Norman, D. G. & Lilley, D. M. The kink-turn motif
111 in RNA is dimorphic, and metal ion-dependent. *RNA* **10**, 254–264 (2004).
- 112 33. Service, R. F. Materials and biology. Nanotechnology takes aim at cancer. *Science*
113 **310**, 1132–1134 (2005).
- 114 34. Holler, N. *et al.* Two adjacent trimeric Fas ligands are required for Fas signaling
115 and formation of a death-inducing signaling complex. *Mol. Cell. Biol.* **23**,
1428–1440 (2003).
- 116 35. Ranzinger, J. *et al.* Nanoscale arrangement of apoptotic ligands reveals a demand
117 for a minimal lateral distance for efficient death receptor activation. *Nano Lett.* **9**,
4240–4245 (2009).
- 118 36. Ban, N., Nissen, P., Hansen, J., Moore, P. B. & Steitz, T. A. The complete atomic
119 structure of the large ribosomal subunit at 2.4 Å resolution. *Science* **289**,
905–920 (2000).
- 120 **Acknowledgements**
- 121 The authors thank R. Furushima, M. Sekiya and Y. Kodama (Japan Science and Technology
122 Agency) for analysis and purification of Tri-RNPs, Y. Fujita (Kyoto University) and
123 M. Takinoue (University of Tokyo) for discussions, and A. Huttenhofer (Innsbruck
124 Medical University) and T.S. Rozhddestvensky (University of Muenster) for providing the
125 L7Ae plasmid. This work was supported by the JST International Cooperative Research
126 Project. Part of the work was supported by the New Energy and Industrial Technology
127 Development Organization (09A02021a).
- 128 **Author contributions**
- 129 H.O., T.K., T.I. and H.S. designed the project. H.O., T.I., S.Y. and H.S. performed AFM.
130 H.O., R.K. and K.E. performed RNP biochemical assays. H.O., S.Y., K.T., T.I. and H.S.
131 evaluated the experimental results. H.O., T.I. and H.S. wrote the manuscript.
- 132 **Additional information**
- 133 The authors declare no competing financial interests. Supplementary information
134 accompanies this paper at www.nature.com/naturenanotechnology. Reprints and
135 permission information is available online at http://npg.nature.com/reprintsandpermissions/
136 Correspondence and requests for materials should be addressed to T.I. and H.S.

Publisher: Nature

Journal: Nature Nanotechnology

Article number: nnano.2010.268

Author (s): Hirohisa Ohno *et al.*

Title of paper: Synthetic RNA–protein complex shaped like an equilateral triangle

Query no.	Query	Response
1	Affiliations 3 and 4 – please provide full postal addresses.	Done. We added full addresses.
2	Please expand acronyms for first use.	Done.
3	Should this be “substituted for”?	Yes. We revised.
4	Please expand IPTG.	Done. (isopropyl β -D-thiogalactoside)
5	BPB and XC expanded OK?	OK.
6	Please expand TBE for first use.	Done. (Tris/Borate/EDTA buffer)
7	Ref 2 – please provide page range.	Done. (1663–1674)
8	Ref 15 – please provide page range, if available.	Done. (833–842)
9	Ref 22 – please provide page range.	Done. (2395–2409)
10	Figure 2 – do you mean upshifted in lanes 7 to 9?	Yes. We modified as follows “in lanes 7 to 9”.
11	Figure 4c, does the lower panel also show data with lower concentrations of metal ions?	Yes. We added a phrase “at lower concentrations of metal ions”.
12		
13		
14		
15		
16		
17		
18		
19		
20		